The Journal of Experimental Biology 201, 2115–2128 (1998)
Printed in Great Britain © The Company of Biologists Limited 1998
JEB1209

THE ELECTRIC IMAGE IN WEAKLY ELECTRIC FISH: PHYSICAL IMAGES OF RESISTIVE OBJECTS IN *GNATHONEMUS PETERSII*

A. A. CAPUTI[1,*], R. BUDELLI[2], K. GRANT[3] AND C. C. BELL[4]

[1]*Division Neuroanatomía Comparada, Instituto de Investigaciones Biológicas Clemente Estable, Avenida Italia 3318, CP 11600, Montevideo, Uruguay,* [2]*Departamento de Biomatemática, Facultad de Ciencias, Universidad de la República, Montevideo, Uruguay,* [3]*Institut Alfred Fessard, CNRS, Gif sur Yvette, France* and [4]*R S Dow Neuroscience Institute, Good Samaritan Hospital, Portland, Oregon, USA*

*e-mail: angel@iibce.edu.uy

Accepted 14 April; published on WWW 25 June 1998

Summary

The present study describes a measurement-based model of electric image generation in the weakly electric mormyrid fish *Gnathonemus petersii*. Measurements of skin impedance, internal resistivity and fish body dimensions have been used to generate an electrical-equivalent model of the fish and to calculate electrical images and equivalent dipole sources for elementary resistive objects. These calculations allow us to understand how exafferent and reafferent signals are sensed by electroreceptors. An object's electric image consists of the modulation of the transcutaneous voltage profile generated by the fish's own discharge. The results suggest a set of rules for electrolocation: (1) the side of the fish where modulation is larger indicates the side on which the object is situated; (2) the object's position in the electroreceptive field is indicated by the point of maximum modulation of the transcutaneous voltage; (3) the degree of focus of the image indicates the distance to the object. In addition, center–surround opposition originating at pre-receptor level is proposed.

Both experimental measurements and modeling indicate that fish skin impedance is relatively low (400–11 000 Ω cm^2) and mainly resistive. This low skin impedance appears to enhance the local electric organ discharge modulation, the center–surround effect, the signal-to-noise ratio for electrolocation and the active space for electrocommunication.

Key words: sensory image, reafference, electroreception, electric fish, model, *Gnathonemus petersii*.

Introduction

Electroreception is a sensory modality that is common in fish and provides an example of parallel evolution in which whole systems of specialized sensory receptors and brain structures have developed for detecting and analyzing naturally occurring electric fields. In addition, in several families of fish, electroreception is accompanied by a set of effector organs and central control pathways specialized for the production of electric signals, which can be detected by electroreceptors. Nearby objects distort the self-generated electric field, allowing these species to actively detect objects that have different conductivities from that of water. The electric image of an object is the modulation that the object causes in the pattern of transepidermal currents. This electric image is analyzed by the central structures of the electrosensory system (Bastian, 1986; Bell, 1989).

Theoretical (Lissmann and Machin, 1958; Heiligenberg, 1973, 1975) and experimental (Boudinot, 1971; Hoshimiya *et al.* 1980; Caputi *et al.* 1989, 1993, 1994; Rasnow *et al.* 1993; Rasnow and Bower, 1996) studies indicate that the electrogenic properties of the electric organ and the post-effector mechanisms [filtering of the electric organ discharge (EOD) by the non-electrogenic tissues] are as important as the impedance of the external object in determining the electric image. The experimental study of the physiology of the electric organ and the impedance of the skin and internal tissues has been an important step in the development of an accurate model of the fish body in the gymnotid fish *Gymnotus carapo* (Caputi and Budelli, 1995). The present study extends this work to mormyrid fish, an African family of weakly electric teleosts.

Mormyrids have several advantages for the modeling of electric images. (1) The electrogenic system is localized to a small and restricted part of the fish body (Bell *et al.* 1976). (2) Behavioral studies indicate that mormyrid fish are able to discriminate between resistive and capacitative impedance (Meyer, 1982; von der Emde, 1991). (3) The ability to detect different types of impedance has been extensively investigated (von der Emde, 1993; von der Emde and Bleckman, 1992). (4) There is extensive literature on the early stages of electrosensory processing (Szabo and Hagiwara, 1967; Szabo and Fessard, 1974; Bennett, 1965, 1971; Zipser and Bennett, 1976*a*,*b*; Bell and Szabo, 1986; Bell, 1981, 1986, 1989,

1990*a*,*b*; Bell and Russell, 1978; Meek and Grant, 1994; Grant *et al.* 1996; Meek *et al.* 1996).

In mormyrids, most of the available data on model parameters derive from experiments in *Gnathonemus petersii*. The electric organ of *G. petersii* was characterized as an electric source by Bell *et al.* (1976). These measurements implied a skin impedance lower than 1 kΩ cm^2. However, this estimate differs from the measurements of skin impedance (50 kΩ cm^2) performed by Bennett (1965), making it necessary to carry out further measurements and to study image generation as a function of skin impedance using the model as a tool.

The longitudinal impedance and the morphological characteristics of the fish body have not been measured previously in this fish family, and such measurements were therefore included in this study.

The data and the model presented here reveal a set of rules for understanding electroreception. The model can be used as a framework for correlating information of different types, including findings from behavioral, physiological, anatomical and theoretical studies. This analytical framework may help to clarify general principles common to other sensory modalities, such as the lateral line (Coombs *et al.* 1996), somatosensory (Keidel, 1984) or visual (Marr, 1982) systems.

Materials and methods

Gnathonemus petersii (*N*=25) were used for this study. When using live fish, all potentially traumatic procedures were carried out under anesthesia, induced either with MS222 (Sandoz; added to the aquarium water at a concentration of 1:10 000, w/v, for rapid induction of anesthesia, followed by 1:30 000, w/v, for continued anesthesia) or Hypnodil (Janssen Pharmaceutica; added to aquarium water at a concentration of 3–5 mg l^{-1}). Where needed, respiration was assisted by running aerated anesthetic solution through a tube inserted into the mouth of the fish, and across the gills, at a perfusion rate of approximately 30 ml min^{-1}.

Fish geometry

Volume, cross-sectional area and skin surface area were estimated as described previously (Caputi and Budelli, 1995).

The volumes of 17 fish ranging from 10 to 20 cm in standard length (defined as the distance from the mouth to the bifurcation of the tail) were measured by water displacement, calculated by adding the fish to a known volume of aquarium water held in a graduated measuring cylinder. Using a similar method, for three fish (10, 13 and 18 cm standard length), the volumes of body portions were measured by lowering the fish headfirst into a measuring cylinder containing a known volume of water, in discrete steps. We obtained a body volume profile by measuring, at each step, the volume of water displaced by the immersed portion of the fish's body, i.e. the volume of the body contained between the tip of the head and a given body cross-sectional plane, defined by the level of the water meniscus along the fish's length at the current step. Experimental data were fitted using a polynomial function of the proportional distance *p* along the fish's length (see Fig. 2). The cross-sectional area at any given level could be calculated as the derivative of the polynomial function.

Skin area was estimated by measuring the perimeter of defined transverse planes in six fish. The perimeter is the spatial derivative of the function relating the skin area to the distance from the head. A polynomial function was fitted to the experimental measurements of body perimeter. Using the mathematical expression obtained, the area of any given body portion could then be calculated. This area is the integral of the polynomial function taken between the transverse planes that define the body portion under study.

To test the hypothesis that fish of different sizes are geometrically similar, three independent tests of similarity were performed. (1) We showed that volume is a linear function of the cube of the fish's standard length. (2) We verified that normalized cross-sectional area (area divided by the square of the standard length) corresponded to the same function of *p*, irrespective of the standard length. (3) We confirmed that normalized perimeter (perimeter divided by standard length) corresponded to the same function of *p*, irrespective of the standard length.

Measurements of the longitidunal impedance of the internal tissues

Deeply anesthetized (MS222, 1:10 000, w/v) fish (standard length between 10 and 18 cm) were maintained in air by perfusing the gills with aerated, high-resistivity (10 kΩ cm) water. A current source was connected between a needle electrode inserted through the lower jaw and a second similar electrode inserted within the caudal 5 % of the tail. Sinusoidal currents (5 μA, 1–10 kHz) were applied, and the voltage drop between two points inside the fish was measured as follows. One recording electrode was placed close to the rostral stimulation electrode, and the second recording electrode was implanted at different successive points along the fish. Under these conditions, the current flow is constant regardless of body cross-sectional area. Consequently, the voltage drop between two points along the fish will be the product of the intensity of the current and the impedance. Thus, we calculated the longitudinal impedance between the jaw and different points along the animal's body from the voltage drop and the applied current. As an additional test for similarity, the normalized resistance (resistance multiplied by standard length) was studied as a function of *p*. We checked the procedure by measuring the resistance of plastic cylinders of different diameters and lengths filled with electrolyte solutions of known conductivity.

Measurements of the fish's skin impedance

Skin impedance was measured in patches of skin in three deeply anesthetized fish maintained in air with perfusion of anesthetic solution across the gills. Two long uninsulated needles were inserted subcutaneously along the entire trunk of the fish. A AgCl-coated silver plate (0.8 cm×0.5 cm or

0.8 cm×0.8 cm) was placed on the outside surface of the skin. A silver wire, insulated except at the tip, was placed between the skin and a piece of filter paper glued to the surface of the silver plate. Sinusoidal stimuli (50 μA peak to peak, at 1 and 10 kHz) were applied between one of the electrodes inside the body and the silver plate. Under these conditions, the current density passing through the skin is the current divided by the area of the silver plate. The voltage drop between the second electrode inside the fish and the silver wire electrode was recorded. These data allowed us to estimate the impedance per unit area of skin. Three to five measurements were performed at each site. In order to estimate the contribution of internal muscle impedance to the measured values, a 1 cm×1 cm piece of skin (which separates easily from the muscle fascia) was gently peeled off at the recording locations using a scalpel, and the experiment was repeated in the absence of the skin. The value for internal muscle impedance could then be subtracted from the initial measurements (skin plus muscle), giving a calculated value for the impedance of skin alone. The skin impedance per square centimeter was calculated as the measured voltage divided by the current density. Mormyrid skin is not uniform all over the body. The region of skin that contains the electroreceptors, the mormyromast epithelium, has a superficial layer of epithelial cells which is not present in the non-mormyromast epithelium (Quinet, 1971). For this reason, we checked for differences in the impedances of mormyromast and non-mormyromast epithelia. After measuring values for mormyromast epithelium, the skin surface was gently rubbed with a cotton swab to remove the superficial layer of epithelial cells, and the experiment was repeated to determine the contribution made by the latter to the impedance of mormyromast epithelium.

The model

The present study extends the approach used by Caputi and Budelli (1995) to construct a model that is able to predict the electric image of objects of different resistance. A box containing the fish, the surrounding medium and the object was modeled as a two-dimensional electric network (Fig. 1A,B). The elements represent the electrical properties of the surrounding medium (including the object), the skin of the fish and the internal tissues. The spatial resolution of the model was 0.5 cm (corresponding to the length represented by each element of the two-dimensional network). Since we modeled a tank 30.5 cm wide and 60.5 cm long, 7381 (=61×121) nodes were defined. Each node of the network connected either two (corners), three (borders) or four (inside the box) elements, situated orthogonally in the same plane, 0.5 cm apart. In order to account for the height of the aquarium, the resistance of the elements was calculated assuming a vertical dimension of 3 cm (Fig. 1A). This models a situation in which the fish is immersed in water 3 cm deep and is in the middle of an aquarium, with the ventral surface of the fish touching the bottom of the aquarium at the middle of the body and the dorsal surface touching the air/water interface. We modeled a 15 cm standard length fish body based on the measurements made in this study (Fig. 1B). Skin resistance was calculated by dividing the measured skin impedance by the skin area in that segment of the fish. Taking into account the thickness of the fish, the resistance between the node inside the fish and the node outside the fish was calculated by adding the skin resistance to the corresponding volume of water. As shown by Caputi and Budelli (1995), the results depend qualitatively and quantitatively on fish size. Most portions of the modeled skin included both mormyromast and non-mormyromast regions but, for the sake of simplicity, skin resistance per unit area was considered to be constant. The simulation was performed with several values of resistance per unit area. The longitudinal internal resistance used in the model was derived from the measurements of this variable in the intact fish.

Experimental measurements showed that the impedance of the skin and internal tissues is resistive and does not have significant capacitative components (see below). Moreover, in contrast to fish of the gymnotid family, the electric organ (EO) in mormyrids is restricted to the tail region. This removes the difficulties associated with a spatially distributed source (Caputi and Budelli, 1995). As a consequence, the fields and currents generated by the EOD in a resistive medium are proportional to the instantaneous EOD amplitude. We therefore simulated the fields and currents generated by a unitary voltage source uniformly distributed along the EO region. To obtain a value for the internal resistance of the source, we measured the longitudinal resistance of the EO in the absence of the EOD. This resistance is similar to the equivalent internal resistance found by Bell *et al.* (1976) for the EOD. When necessary, we calculated the fields and sources by multiplying the results obtained using a unitary source by the instantaneous value of the EOD electromotive force (based on the measurements of Bell *et al.* 1976).

For each node of the network, we defined an equation according to the node's Kirchoff's law; individual intensities were calculated according to Ohm's law (Fig. 1C). The resulting system of equations, in which the unknowns are the node voltages, is undetermined since the voltages are related to an arbitrary zero. To remove this problem, we eliminated one equation and assigned a zero voltage to one of the nodes at a corner. This system of equations was then solved by Cramer's (Cramer, 1960) method using MATLAB.

We studied the effects of objects on the magnitude and distribution of the transcutaneous voltage and current density. Disparity between our experimental measurements of skin resistance and those of Bennett (1965) induced us to study image generation as a function of skin resistance, using the model as a tool.

Results

Morphological characteristics of Gnathonemus petersii

Individual fish of this species are geometrically similar, making it possible to generalize the model for fish of different standard length. Geometrical similarity requires that distances in different individuals are proportional to fish length, areas are

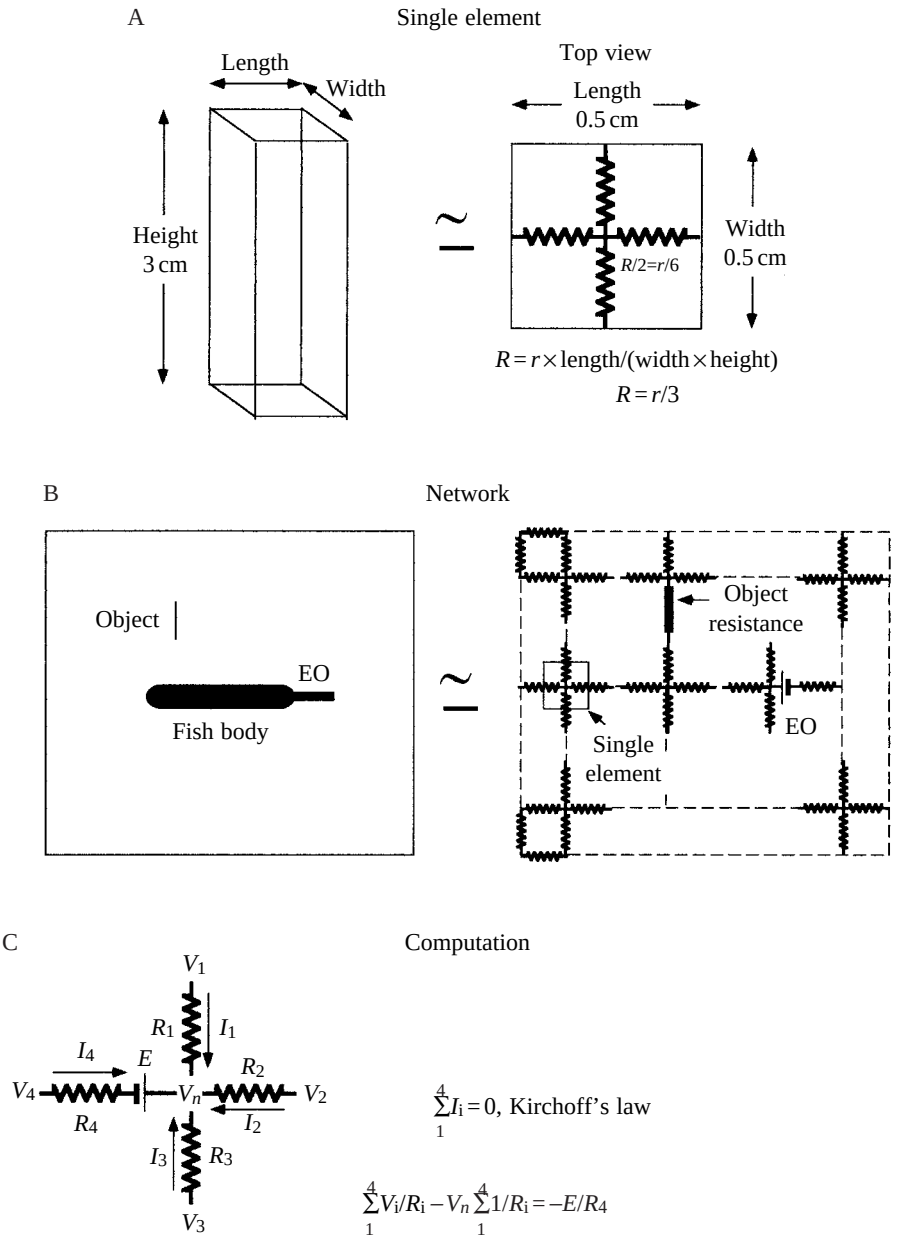

Fig. 1. Modeling procedure. (A) The modeled volume (30.5 cm×60.5 cm×3 cm) was divided into rectangular prisms each of 0.5 cm×0.5 cm×3 cm. Each of these prisms was considered as having uniform resistivity (ρ) and is represented in two dimensions as four resistors. (B) The fish, water and object were represented by an electrical network (*E*, electric organ equivalent electromotive force). (C) Computation was carried out according to Kirchoff's law. A system of 7381 linear equations was defined, one for each node. The system of equations was solved using Cramer's method. V_1–V_4, voltages at the four nodes; R_1–R_4, resistances between the nodes; I_1–I_4, current through the resistances; *n*, node number; *i*, index (1–4); EO, electric organ.

proportional to the square of fish length and volumes are proportional to the cube of fish length (Caputi and Budelli, 1995; Fig. 2A). We also tested geometrical similarity by verifying that the following parameters were independent of fish length after normalization: (1) normalized cross-sectional area obtained by dividing the measured cross-sectional area at a given position by the square of the length; (2) normalized perimeter obtained by dividing the measured perimeter at a given position by the length; and (3) normalized resistance of given segment of the fish obtained by multiplying the measured resistance of that segment by the length (since resistance will increase with fish length but decrease with cross-sectional area, which is in turn proportional to the square of the length).

In Fig. 2B–D, normalized cross-sectional area, perimeter and longitudinal resistance are plotted as a function of *p* (percentage of standard body length). Because of geometrical similarities, these plots show that the same function of *p* is a good estimator of each variable considered, even for fish of different length. Thus, these plots enable us to determine an expression for each normalized variable as a function of the distance to the head. To derive these expressions, the pooled data from different fish were fitted with a polynomial function using the least-squares method.

Measurements of the longitudinal impedance

As in the previous study of *Gymnotus carapo* (Caputi and Budelli, 1995), no significant phase difference between the stimulating current and the recorded voltage drop was found, indicating the lack of a significant capacitative component of the internal impedance. In addition, no difference was found between the impedance at 10 kHz and 1 kHz, which also indicates the lack of a capacitative component. The quotient of

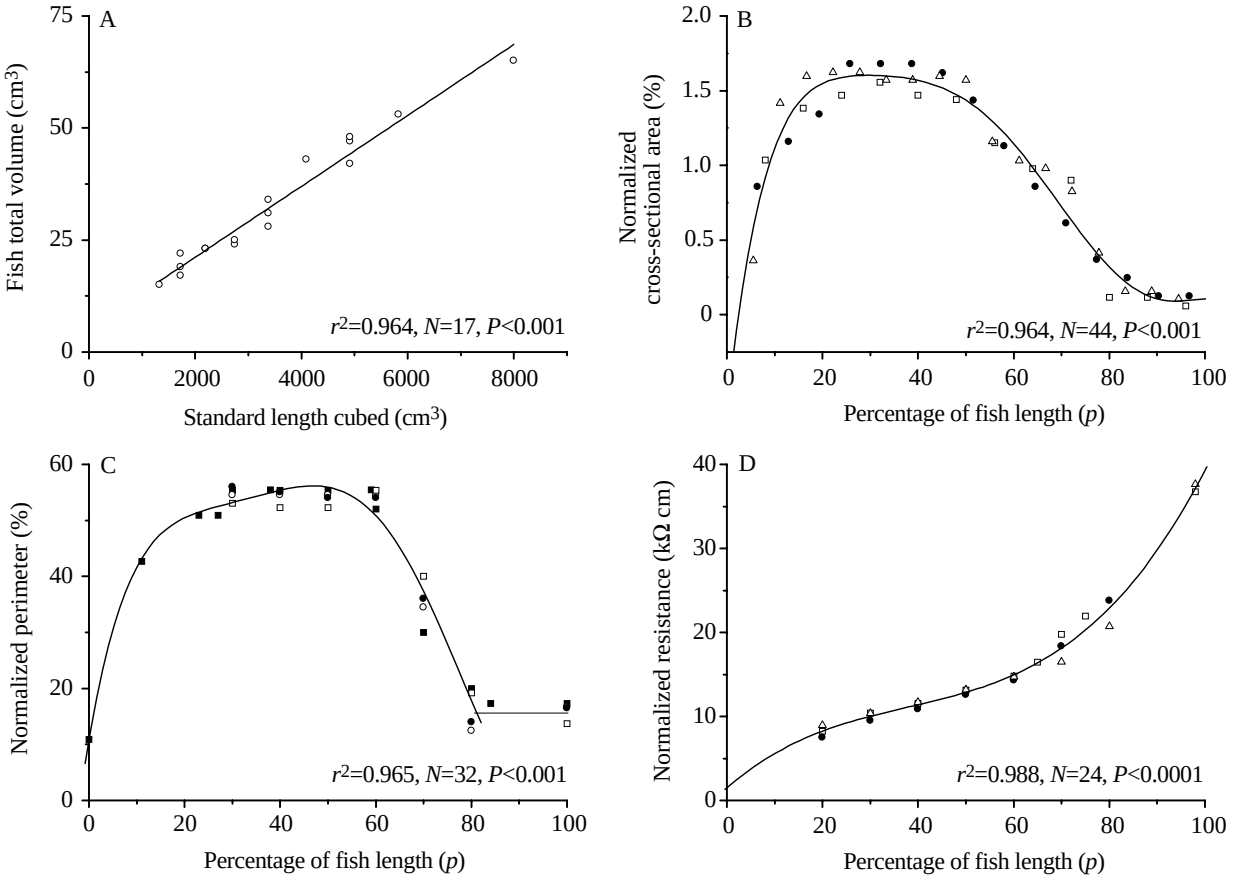

Fig. 2. (A) Fish volume as function of the cube of body length. The equation for the line is: $v=5+0.008L^3$, where v is volume and L is standard length. Each open circle corresponds to one fish. (B) Normalized cross-sectional area (100 × area divided by the square of the fish standard length) at different points along the fish body; p is the percentage distance from the mouth, where the standard length, from the mouth to the bifurcation of the tail, equals 100 %. Data are from three fish of 10.5, 13 and 18 cm standard length. The equation for the polynomial function of p is: $y=-0.64-0.30p-16\times10^{-3}p^2+46\times10^{-5}p^3-7\times10^{-6}p^4+53\times10^{-9}p^5-15\times10^{-11}p^6$. Different symbols correspond to fish of different standard length; open squares, 10.5 cm; filled circles, 13 cm; open triangles, 18 cm. (C) Normalized perimeter (100 × perimeter divided by fish length) as a function of p. Data are from four fish ranging from 11 to 15 cm in standard length. The equation for the polynomial function of p is: $y=0.32+0.36p-38\times10^{-4}p^2-4\times10^{-4}p^3+16\times10^{-6}p^4-22\times10^{-8}p^5+10^{-9}p^6$. Different symbols correspond to fish of different standard length; filled squares, 11 cm; open circles, 13 cm; filled circles, 14 cm; open squares, 15 cm. (D) Longitudinal normalized resistance (resistance multiplied by fish length) of body segments between the mouth and a given point as function of p. The mathematical expression for the normalized resistance as a function of p is: $y=3.6+0.32p-55\times10^{-4}p^2+57\times10^{-6}p^3$. Different symbols correspond to fish of different standard length; open squares, 10.5 cm; filled circles, 13 cm; open triangles, 18 cm.

voltage and current was therefore used to calculate the longitudinal impedance. Since this impedance is predominantly resistive, the term 'longitudinal resistance' is generally used below.

Fig. 2D shows the experimentally measured normalized longitudinal resistance from the jaw to different positions along the fish body, expressed as a function of p. When resistance was normalized for length, all values fell on the same curve. We fitted a third-order polynomial function to the data ($P<0.0001$, $r=0.988$, $N=24$), allowing the resistance of a given body portion to be calculated.

Measurements of skin impedance

We determined the specific impedance of known skin areas by measuring the voltage drop generated by sinusoidal currents (Fig. 3). Little phase shift was observed, indicating that the skin impedance is mainly resistive. The ratio between the voltages recorded at the same site at 1 and 10 kHz was 1.33±0.16 ($N=14$) for the mormyromast epithelium, 1.27±0.04 ($N=11$) for the non-mormyromast epithelium and 1.19±0.17 ($N=3$) (means ± S.E.M.) for the muscular tissue.

The mormyromast region, on the back, head and belly, contains electroreceptors and is covered by a clear outer layer of tightly packed epithelial cells. The non-mormyromast region, on the flanks, has no electroreceptors and no external layer of epithelial cells (Quinet, 1971). Individual measurements varied from 2180 to 14 500 Ω cm^2 for the dorsal mormyromast epithelium (6056±0.828 Ω cm^2, $N=18$), from 470 to 5850 Ω cm^2 for the ventral mormyromast epithelium (2024±0.403 Ω cm^2, $N=13$) and from 400 to 1100 Ω cm^2 for the

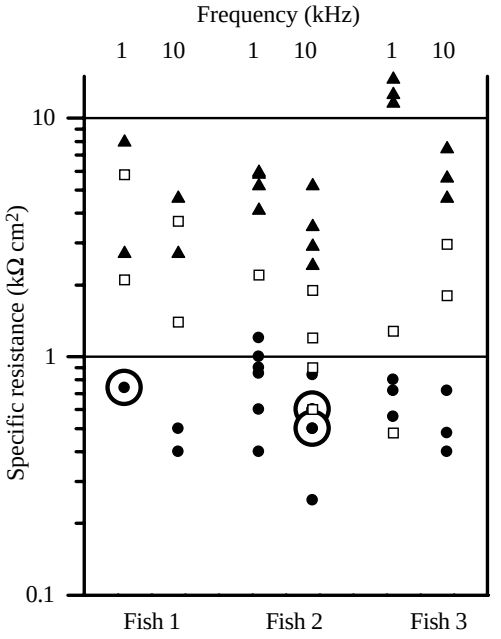

Fig. 3. Specific resistance of the skin. Skin specific resistance was determined at different regions and at frequencies of 1 and 10 kHz in three fish of 13, 14 and 15 cm standard length. The regions were classified as: dorsal mormyromast epithelium (filled triangles), ventral mormyromast epithelium (open squares) and non-mormyromast epithelium (filled circles). Large open circles indicate one or more points superimposed.

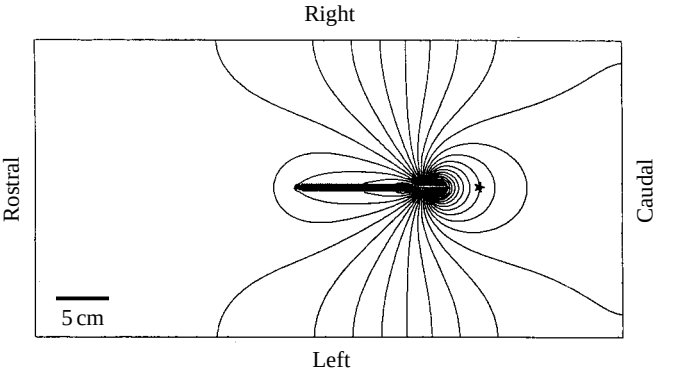

Fig. 4. Simulation of the field potential generated in a homogeneous medium. The field potential was calculated assuming a mean skin resistance of 1 kΩ cm^2 and a water resistivity of 10 kΩ cm. The box represents the simulated tank. The star indicates the isopotential line separating inward and outward currents at the fish skin. Isopotential lines represent equally spaced field values. The fish (15 cm standard length) is shown shaded in the center of the tank.

non-mormyromast epithelium (650±0.226 Ω cm^2, N=22) (means ± S.E.M.). When the external layer of epithelial cells covering the mormyromast epithelium was removed, the mormyromast epithelium impedance decreased to within the range for the non-mormyromast epithelium.

From these measured values, we were able to calculate the values of resistance, capacitance and the time constant of the skin. Values for dorsal mormyromast, ventral mormyromast and non-mormyromast epithelium resistances were, respectively: 6335 Ω cm^2, 1810 Ω cm^2 and 363 Ω cm^2. The time constant was always less than 15 μs and the capacitance less than 45 nF cm^{-2}. Since the power spectrum of the EOD is concentrated below 10 kHz (Moller, 1995), this result indicates that the effect of skin capacitance is negligible. Therefore, we will refer below to the skin impedance as skin resistance.

Our results differ by at least an order of magnitude from the estimate of 50 kΩ cm^2 for skin resistance reported by Bennett (1965). This disparity in experimental measurements made it necessary to study image generation as a function of skin resistance using the model as a tool (see Figs 6, 11–13).

The skin resistance of a longitudinal section of the fish is the specific skin resistance divided by the skin area. The skin area between two given cross-sectional planes is the integral of the perimeter function. We calculated the skin area of any given portion of the fish by integrating the polynomial function obtained from perimeter measurements (Fig. 2C). Since the vertical dimension was compacted, specific resistance differences among epithelial types were neglected. However, we took into consideration the areas and specific resistances to calculate (by weighted average) the values of specific resistance used for modeling calculations.

Results from the model

Electric fields in a homogeneous medium

Fig. 4 shows the field potentials generated by a 15 cm standard length fish located in the center of a 60.5 cm×30.5 cm×3 cm tank filled with water with a resistivity of 10 kΩ cm. Since potentials and currents are proportional to the EOD, simulations were performed by substituting a unitary source located in the tail of the fish for the EOD. The resistivity of the internal tissue is much lower than that of the water, and the internal currents therefore tend to follow the longitudinal dimension of the fish body. They take a transverse direction across the skin of the fish in its immediate environment. Consequently, over the electroreceptive surface, the isopotential lines close to the fish tend to be parallel to the skin.

The head-to-tail peak-to-peak EOD in a homogeneous medium (2 kΩ cm) is approximately 6 V (Bell *et al.* 1976). Model calculations based on an electromotive force of 24 V peak to peak and a mean skin resistance of 500 Ω cm^2 reproduced the value of 6 V obtained by Bell *et al.* (1976). For skin resistances of 5 kΩ cm^2 and 50 kΩ cm^2, the head-to-tail EOD potential differences would be 1.7 V and 0.4 V, respectively.

Electroreceptors are stimulated by transcutaneous voltages or currents during the EOD. We present our results as transcutaneous voltage profiles, rather than as transcutaneous currents, in order to allow comparison with voltage measurements of the dynamic range of mormyromast receptors determined by Bennett (1965), Bell (1990*b*) and von der Emde (1993). In the absence of objects, the transcutaneous voltage constitutes a reference signal that we call the basal stimulus.

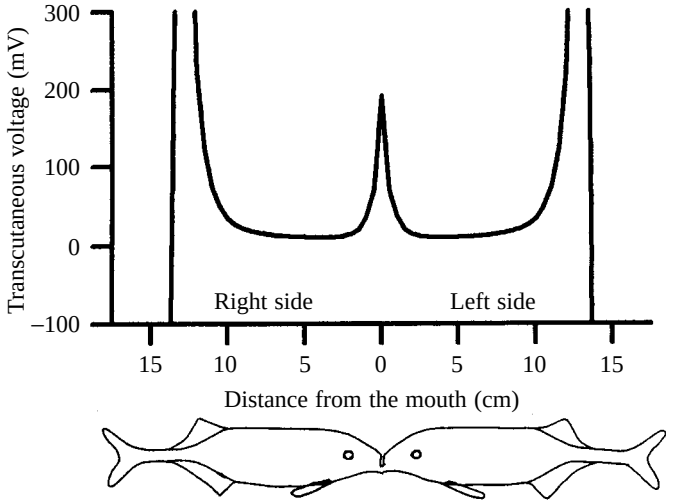

Fig. 5. Transcutaneous voltages. The transcutaneous voltage profile was calculated under the same conditions as in Fig. 3. The abscissa represents distance along both sides of the fish's skin, as shown in the diagram. The zero value corresponds to the mouth. Note that this graph corresponds to a bounded continuous function: the ordinate scale was selected to show the variation of voltages in the electroreceptive zone.

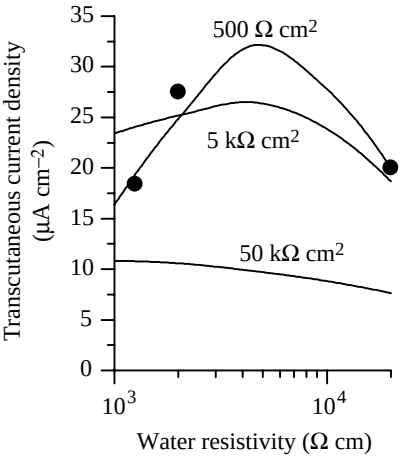

Fig. 6. Transcutaneous current density as function of water resistivity. Continuous lines correspond to simulated current densities for three values of skin resistance. Filled circles represent values calculated from Fig. 6 in von der Emde (1993).

In the presence of objects, an electric image results from the modulation of this basal stimulus. Thus, knowledge of the basal transcutaneous voltage is important for studying image generation.

Fig. 5 shows the transcutaneous voltage calculated under the same conditions as Fig. 4. Although transcutaneous voltage decreases from caudal to rostral sites along the fish body, it increases in the head, where most electroreceptors are located. This result, although interesting, may derive partially from an artificial edge effect at the rostral pole of the fish body since fields shapes are quantitatively different in two and three dimensions. In addition, the resolution of the model is not sufficient to represent the submandibular organ, the mouth and the gills. When a low-resistance path representing the mouth and gills was included, the edge effect was attenuated without changes in transcutaneous voltages for the rest of the fish body. Further constructions of electrical images were made in the uniform region of the trunk to avoid these difficulties with the most rostral region.

The relationship between skin and internal resistance determines the spatial filtering properties of the fish's body. The model can be used to study the transcutaneous current density as a function of the skin resistance and water resistivity. Simulation results were compared with those obtained from von der Emde's (1993) data, based on direct measurements of the local EOD. Fig. 6 shows that the simulations with low skin resistance ($500\,\Omega\,cm^2$ or $5\,k\Omega\,cm^2$) fit the experimental results better than those assuming a higher skin resistance ($50\,k\Omega\,cm^2$). Furthermore, the flat profile obtained with a resistance of $50\,k\Omega\,cm^2$ is not compatible with the reduction in the response of electroreceptors observed by Bell and Russell (1978) when water resistivity was lowered below $10\,k\Omega\,cm$. The peak in the $500\,\Omega\,cm^2$ curve is due to two causes. (1) For low skin and water resistance, the current produced by the electromotive force tends to flow close to the tail. Consequently, the current density in the rostral half of the fish decreases when the water resistivity decreases. (2) At higher water resistivities, the total current produced by the electromotive force depends strongly on the water resistivity. Thus, an increase in the water resistivity produces a decrease in the current density.

Electric image of a resistive object

The elements of the fish body model are resistors, and the spatial location of the source remains fixed throughout the duration of the EOD. Thus, when purely resistive objects are in the environment, the currents that flow around the fish and back through the skin can be calculated from the instantaneous value of the EOD and model resistors. Fields and currents appear instantaneously and vary in proportion to the instantaneous value of the EOD. As pointed out by Lissmann and Machin (1958) and Bacher (1983), resistive objects modify the electric field in the same way as an equivalent dipole whose moment depends on (1) the amplitude of the EOD, (2) the impedance and the position of the object, and (3) water resistivity.

A resistive object may be represented in the model by changes in the resistance of individual elements with regard to the water. For simplicity, we consider below an 'elemental object' (i.e. a change in resistance between two adjacent nodes in the external medium). For such an object, the magnitude of the equivalent dipole may be calculated as the drop in voltage across the object minus the drop in voltage at the same sites in the absence of the object:

$$D = E_e R_e (R_o - R_w)/[(R_e + R_w)(R_o + R_e)]\,,$$

where D is the value of the object-equivalent dipole, R_o is the

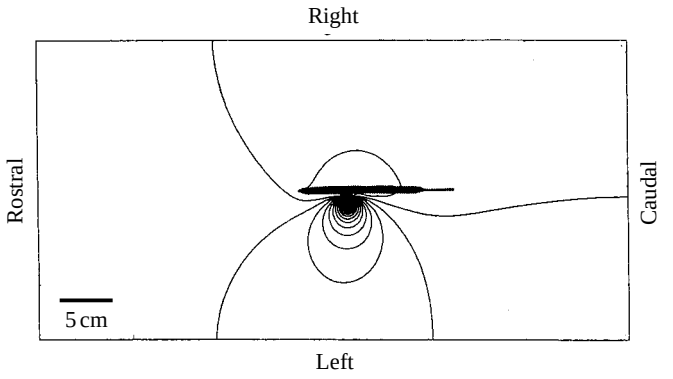

Fig. 7. The field potential generated by a short circuit. Simulated field potentials produced by a vertically oriented highly conductive plate, 1 cm×3 cm (width × height), located perpendicular to the skin, 0.75 cm lateral to the midline and 5.5 cm caudal to the mouth on the left side of the fish are represented as in Fig. 4 (water resistivity 10 kΩ cm, skin resistance 1 kΩ cm^2). The field shown was calculated as the difference between the fields produced by the electric organ discharge in the presence and in the absence of the object. Note that isopotential lines accumulate on the object side.

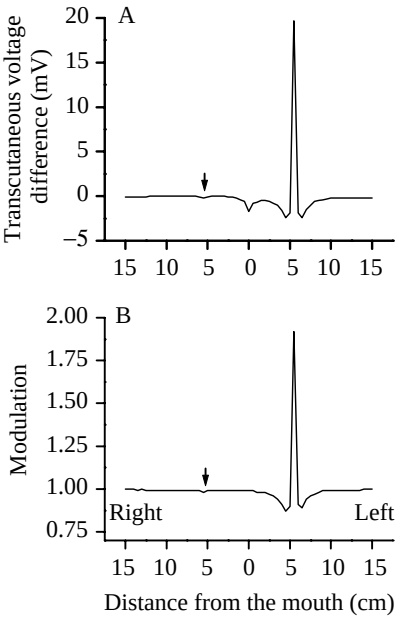

Fig. 8. Transcutaneous voltage difference (A) and modulation (B). The transcutaneous voltage difference is the difference between the transcutaneous voltage profiles in the presence and in the absence of the object. Modulation is the quotient of the transcutaneous voltage profiles in the presence and in the absence of the object (same conditions as in Fig. 7). Arrows indicate the object image on the contralateral side. The abscissa represents distances along both sides of the fish's skin (see Fig. 5). The zero value corresponds to the mouth.

resistance of the object, R_w is the resistance of a water element. E_e and R_e are, respectively, the equivalent electromotive force and series resistance of the fish source as 'seen' from the object, according to Thevenin's theorem. This theorem states that all linear networks can be represented by an equivalent electromotive force and an equivalent series resistance. Considering all the elements in the system, except the object, as an electrical network, we can represent them by E_e and R_e, respectively. E_e is proportional to the EOD, and the sign of D depends on the relative conductance of the object with regard to the water. E_e and R_e will depend on the position and orientation of the object in relation to the fish.

The electric image produced by a short circuit is equivalent to the image produced by a plate of very low resistance with the same orientation. The value of the equivalent dipole for a short circuit corresponds to the value of D when R_o is zero. A short circuit between two points in the surrounding water has been used extensively as an experimental tool for exploring the electrosensory system. Fig. 7 shows the perturbation of the simulated field resulting from such a short circuit. Since the distance between adjacent equipotential lines is reciprocally related to the local field, most effects of objects are concentrated close to their mass. The perturbation of the field on the opposite side of the fish is very small. This 'shielding' effect results from the low resistance of the internal tissues.

Fig. 8A shows the difference between the transcutaneous voltage in the presence of the object and the transcutaneous voltage in the absence of the object under the same conditions as in Fig. 7. Fig. 8B shows the modulation of the basal transcutaneous voltage produced by the object. Modulation is defined as the transcutaneous voltage in the presence of the object divided by the transcutaneous voltage in its absence. During active electroreception, the sensory afferents are driven continuously by the basal transcutaneous voltage; therefore, it seems reasonable to take the basal transcutaneous voltage as the baseline stimulus.

There is a small negative peak at the mouth (distance 0 cm in the graph) for the voltage difference (with object minus without object), but no such peak appeared in the modulation. As this effect is present with the same intensity when the source is inside (the EOD) and outside (the equivalent dipole of the object) the fish, it is eliminated when modulation is calculated. In contrast, all other peaks in the voltage difference plot are also found in the modulation plot. Consequently, the amplitude of the modulation indicates the magnitude of the perceived stimulus.

The general features of transcutaneous voltage profiles in the presence of a short circuit are as follows. (1) The maximum occurs at the point on the skin closest to the object. (2) Most of the perturbation occurs on the side of the skin closest to the stimulus, as expected from the field plots. (3) The magnitude and direction of the perturbation vary along the fish, depending on the position of the object. (4) The region of the increase in amplitude of the transcutaneous voltage at the point on the skin closest to the object (center region) is surrounded by regions of decreased amplitude (surround region) with regard to the basal transcutaneous voltage. This particular pattern will be referred to below as a 'Mexican hat' effect. Similar results were obtained by Scheich and Bullock (1974) in gymnotoid fish. This spatial pattern of currents is reflected in the activity

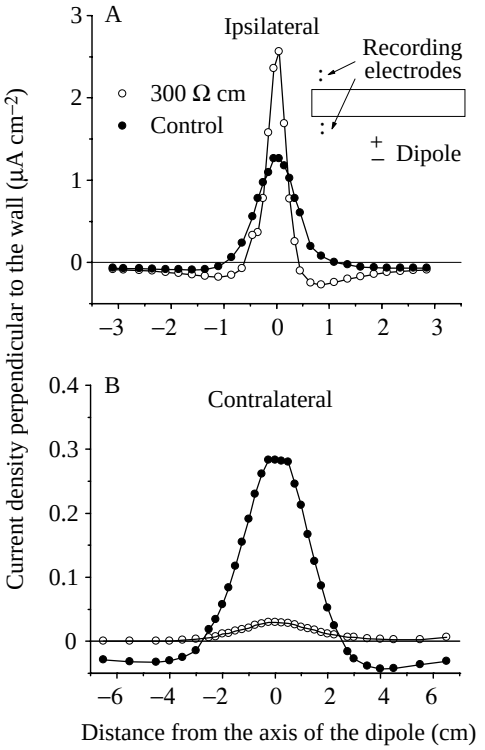

Fig. 9. Reproduction of predictions using a model fish. A physical model fish (a 15 cm×1 cm×3 cm, length × width × height, agar bock with a resistivity of 300 Ω cm) was placed in a dipole field generated in a water tank (52 cm×36 cm×10 cm, length × width × height, resistivity 10 kΩ cm). The agar block was placed in the center of the tank with the dipole oriented perpendicular to its lateral surface at a distance of 1.25 cm. The voltage drop between two electrodes (0.5 cm apart, oriented perpendicularly, see inset in A) was measured at different distances from the dipole axis along both sides of the agar block; A, ipsilateral; B, contralateral. The current density (open circles) was calculated taking into account the water resistivity (10 kΩ cm). Control (filled circles) experiments were performed in the absence of the agar block.

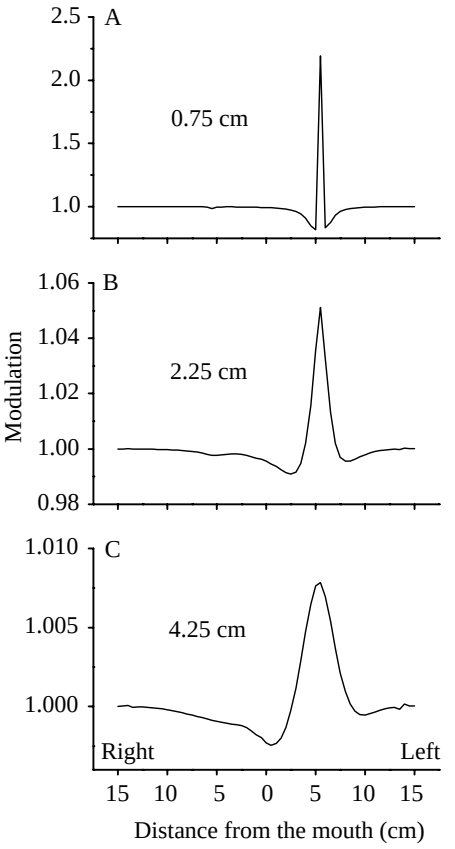

Fig. 10. Transcutaneous voltage modulation for different object distances. Simulated modulation profiles resulting from an object-equivalent dipole situated at three different distances (A–C) perpendicular to the fish body (same conditions as in Fig. 7). Note that, when the distance is greater, the peak and its flanking troughs are wider. The abscissa represents distances along both sides of the fish's skin (see Fig. 5). The zero value corresponds to the mouth.

pattern of electroreceptors when stimulated by conductive and non-conductive objects (Szabo and Hagiwara, 1967).

To confirm that the model results are preserved qualitatively in three dimensions, we performed a simple physical control experiment in which the drop in voltage produced by a dipole along both sides of an agar model fish placed in a tank was measured. In Fig. 9, these results are compared with measurements made at the same points within the tank in the absence of the agar model fish. The Mexican hat effect was enhanced on the side ipsilateral to the dipole (Fig. 9A), and a notable shielding effect was observed on the contralateral side (Fig. 9B). An additional conclusion from this experiment is that both the Mexican hat effect and the shielding effect can be explained by an internal fish resistivity lower than the water resistivity.

Fig. 10 shows the modulation profiles produced by a short circuit at different distances from the mid-sagittal plane of the fish. The peak amplitude of the image is perceived at the ipsilateral skin region in front of the object, and this decays as a negative power function of the object distance (with an exponent of approximately –2.9). The peak width and the width of the troughs flanking it increase with increasing distance between the short circuit and the fish. At the same time, the transitions between the peak and the surrounding troughs become smoother.

Fig. 11 shows the transcutaneous voltage difference profiles produced by a short circuit 5.5 cm caudal to the mouth and 0.5 cm from the skin, calculated for different skin resistances. The amplitude of the basal transcutaneous voltage increases monotonically with increasing skin resistance (Fig. 12A). However, the amplitude of the transcutaneous voltage difference increases only up to a maximum at a skin resistance of 10 kΩ cm^2, after which it decreases (Fig. 12B). Modulation decreases monotonically with skin resistance (Fig. 12C).

In order to analyze further features of the the electric image from the point of view of electroreceptors, we plotted the local transcutaneous voltages corresponding to a homogeneous medium (Fig. 13, basal stimulus) and the limits of the transcutaneous voltage modulation as a function of skin

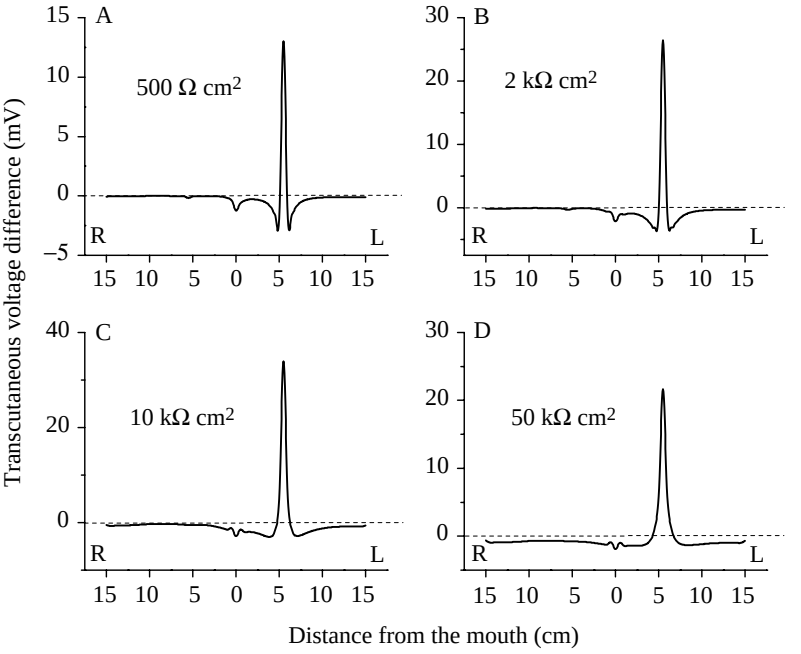

Fig. 11. Transcutaneous voltage differences for different skin resistances. Simulated profiles obtained using skin resistances of 0.5, 2, 10 and 50 kΩ cm^2 (same conditions as in Fig. 7). The abscissa represents distances along both sides of the fish's skin (see Fig. 5). The zero value corresponds to the mouth. L, left; R, right.

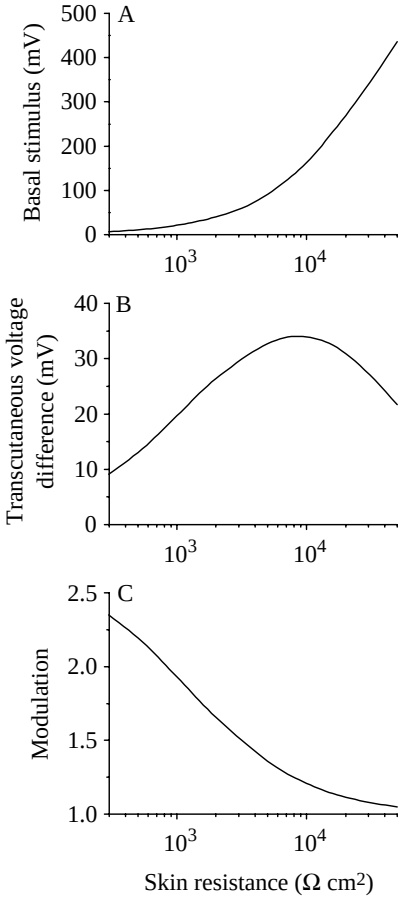

Fig. 12. Transcutaneous voltage (A), transcutaneous voltage differences (B) and transcutaneous modulation (C) as a function of skin resistance. Same conditions as in Fig. 7.

resistance. These limits correspond to two extreme situations: a short circuit (Fig. 13, very conductive object) and a very large resistance (Fig. 13, non-conductive object). Receptors with thresholds above the line for the very conductive object would not be stimulated and would always be silent. Receptors with thresholds one dynamic range below the line for the non-conductive object would always show a saturated response. Using data from Hopkins (1981, 1983) and Bell (1990*b*), we take 6 dB as an approximate value for the dynamic range of mormyromast electroreceptors. Accordingly, a saturation zone is drawn 6 dB below the lower limit of the modulation range in Fig. 13. Receptors with thresholds in this lower shaded area would be saturated by the minimum possible reafferent transcutaneous voltage. Thus, in order to be functionally effective, receptors coding for resistive objects must have their threshold in the non-shaded area.

We used previously reported data to analyze how electroreceptors would perform for different skin resistances. The mormyromast range of thresholds was determined by several authors. Bennett (1965) and Bell (1989, 1990*a*,*b*) determined the transcutaneous voltage thresholds, and von der Emde and Bleckmann (1992) determined the external field threshold (which corresponds to the transcutaneous current). In Bennett's (1965) study, the threshold ranged between 3 and 50 mV for long-duration rectangular waves. Bell (1989, 1990*a*,*b*) used EOD-like, initially negative, sine waves of 5 kHz and found that thresholds for type B receptors ranged from 25 to 100 mV and that thresholds for type A receptors ranged from 15 to 220 mV for these stimuli. These ranges are indicated with horizontal lines in Fig. 13 (A and B). At skin resistances higher than 30 kΩ cm^2, all the type B receptors would be saturated and the type A receptors would be either saturated or working in a reduced part of their dynamic range.

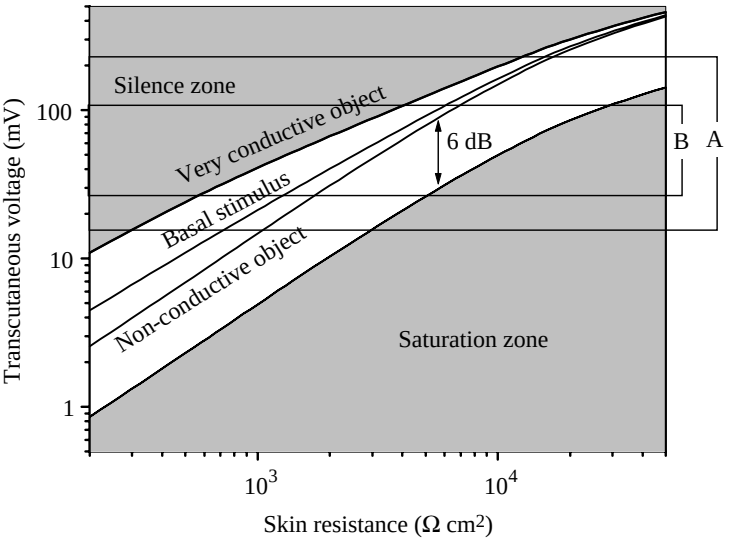

Fig. 13. Transcutaneous voltage as a function of skin resistance. The basal stimulus line represents the local transcutaneous voltage in a homogeneous medium. The modulation range around this line was calculated for a small object 0.75 cm from the midline and 5.5 cm from the mouth. This range corresponds to the area limited by the lines for the very conductive object and the non-conductive object. Receptors with thresholds falling within the shaded area drawn 6 dB below the open-circuit line would be saturated irrespective of the resistance of the object. Receptors with thresholds falling within the shaded area above the short-circuit line would be silent irrespective of the resistance of the object. At a skin resistance greater than 30 kΩ cm^2, all the type B receptors (threshold voltages between 25 and 100 mV) would be saturated and all the type A receptors (threshold voltages between 15 and 220 mV) would be working in a reduced part of their dynamic range. In contrast, between 3.8 and 5 kΩ cm^2, all the type B receptors and a majority of the type A receptors would be working within their dynamic range.

In contrast, between 3.8 and 5 kΩ cm^2, all the type B receptors and a majority of the type A receptors would be working within their dynamic range. This possibility is functionally the most likely, and thus the results obtained from this kind of analysis add further support to our finding that skin resistance is relatively low.

Discussion

The present study provides a framework for correlating behavioral, physiological, anatomical and theoretical results on electrolocation in mormyrid fish. Calculations of the electric images (i.e. transcutaneous voltage profiles) under different conditions allow us to understand the perception of objects that disturb the fish's own electric field (reafferent signals) as well as the formation of images arising from externally generated fields (exafferent signals).

Active electroreception may be conceived as the generation of currents by virtual dipoles equivalent to the stimulus object (Lissmann and Machin, 1958; Bacher, 1983; Rasnow, 1996). These dipoles reproduce the distortion caused by the object in the basal field generated by the EOD. In the case of resistive objects, the magnitudes of these dipoles are proportional to the magnitude of the basal field at the site of the object and, consequently, to the EOD amplitude. The polarity of the equivalent dipoles depends on whether the object has a resistivity larger or smaller than that of the water.

The determination of the electric image of an object was made in two steps: (1) calculation of the equivalent dipole for an elemental resistive object located outside the fish, and (2) calculation of the transcutaneous voltage profiles caused by the dipole.

Two features simplified the task of image calculation still further. The fields and transcutaneous voltages produced by dipoles are proportional to the dipole magnitude, and the fields and transcutaneous voltages produced by a set of dipoles are equal to the sum of the effects produced by the individual dipoles. Thus, the field, basal transcutaneous voltage and object-equivalent dipole magnitudes are proportional to the amplitude of the EOD. In addition, tissues are mainly resistive and, since we are considering only resistive objects, no phase lags are involved and the results at any instant are independent of the results at any previous instant.

Limitations of the model

A first set of limitations of this model derives from the assessment of impedance distribution within the fish. According to previous arguments, knowledge of the spatial distribution of impedance is crucial for accurate image calculation. Our theoretical fish lacks anatomical details, in particular in the head region. Taking into account that the spatial resolution in our model was limited to 0.5 cm, it was not possible to represent details of fish anatomy, thus generating distortions close to the rostral pole where most electroreceptors are located. Smoothing of the rostral pole and ignoring features such as the gills, submandibular organ, lateral line canals and mouth may lead to overestimation of the amplitude of the transcutaneous voltages at the rostral pole.

Another limitation was the use of a constant skin resistance per unit area, thus disregarding the vertical distribution of resistance and transcutaneous voltage. This may introduce errors, particularly in regions where the vertical dimension of the fish is less than the depth of the tank.

Since both limitations described above affect the currents at the rostral pole, we have made quantitative comparisons by referring to electric images calculated for the more uniform trunk region.

A third set of limitations may result from basing the model calculations on purely resistive objects. This point will be explored further in a future study of the electric images of capacitative objects (R. Budelli and A. A. Caputi, in preparation).

Despite these limitations, the model reproduces quite accurately the general features and the orders of magnitude of

parameters which contribute to the formation of electric images, and it will be of significant value in future studies of the neural encoding of stimulus objects. Precise determination of the electric image is precluded by the limitations discussed above, but the present model strategy can be combined with more precise measurements of fish geometry and a large amount of computation power to achieve very precise electric images.

Nevertheless, construction of a very complete image including the detailed irregular geometry of the fish's body or the inhomegeneity of stimulus objects might, in fact, unnecessarily complicate the general picture and cloud our understanding of the basic principles of electric image formation (Borges, 1967).

Importance of skin impedance

Since the measurements made by Bennett (1965), it has been assumed that mormyrids have a high skin impedance and that this is necessary for active electroreception. Here, we present measurements indicating that skin resistance is at least one order of magnitude lower than that determined by Bennett (1965), and our modeling supports this conclusion, indicating that active and passive electric imaging would benefit from relatively low skin resistance.

Bell *et al.* (1976) determined the skin impedance of two patches of skin connected in series with the EO. Since the area of these patches was approximately 0.5 cm^2 and their impedance was 2–2.8 kΩ, we can infer a skin impedance of between 500 and 700 $\Omega\,cm^2$. Our measurements yielded values in the range 400–11 000 $\Omega\,cm^2$, depending on the region of the skin and the fish. Skin resistance measurements at different regions of the fish skin represent the first attempt to provide an accurate picture of this important parameter. The results show a clear difference between the three types of skin. Skin resistances are approximately 10 times greater in the dorsal mormyromast epithelium (mean 6056 $\Omega\,cm^2$) than in the non-mormyromast epithelium (mean 650 $\Omega\,cm^2$), while the resistance of ventral mormyromast epithelium is intermediate (mean 2024 $\Omega\,cm^2$).

The mormyromast region is covered by a clear outer layer of tightly packed epithelial cells. Removing the external layer of epithelial cells lowered the mormyromast epithelium resistance to within the range for the non-mormyromast epithelium, indicating that this layer of cells constitutes an important resistive element. This explains the measured differences between mormyromast and non-mormyromast epithelia, although variations within the mormyromast epithelia and their possible functional significance remain unexplained.

In addition, the model provides several indirect indications that mean skin resistance is relatively low. Experimental results from other investigators fit our calculations based on low skin resistance, but would not support those based on high skin resistance. (1) The amplitude of the head-to-tail EOD is approximately 6 V (Bell *et al.* 1976). Calculations based on an electromotive force of 24 V peak to peak give a head-to-tail EOD amplitude of 6 V for a skin resistance of 500 $\Omega\,cm^2$. For a skin resistance of 50 kΩ cm^2, the head-to-tail EOD amplitude is only 0.4 V. (2) The plot of transcutaneous current density as a function of water resistivity obtained from von der Emde (1993) show a peak at intermediate values of water resistivity. These experimental data fit the model calculations based on low skin resistance. (3) The decrease in electroreceptor response with decreases in water resistivity reported by Bell and Russell (1978) indicates a reduction in the image amplitude. This reduction is obtained only when model calculations are based on low skin resistance values.

Finally, the following theoretical arguments suggest that low values of skin resistance are best suited for electrocommunication and electrolocation. (1) The current delivered to the medium decreases as skin resistance increases. An increase in skin resistance would also increase the distance along the body between the sources and sinks of the current generated by the fish, thus increasing the distance between equivalent poles. But the effect of an increase in dipole distance on dipole moment would be smaller than the effect of reducing the amount of current injected into the medium. Thus, the active space would also decrease with increasing skin resistance. (2) Modulation of the local EOD by a short circuit decreases with skin resistance from 1.5 (at 500 $\Omega\,cm^2$) to 0.2 (at 50 kΩ cm^2). (3) The 'Mexican hat' profile is sharper for low skin resistance. This and the dependence of modulation on skin resistance both contribute to improving the contrast of the image at low skin resistance.

Implications of geometrical similarity

Geometrical similarity allows us to describe any fish body on the basis of a few variable and thus facilitates modeling. However, the model results will still depend in a relatively complex way on fish size (Caputi and Budelli, 1995). For example, the size of the 'Mexican hat' effect for a fish of a given length can only be determined by simulating the transcutaneous currents for that particular body length. Objects of similar size and a similar distance from the fish will produce different images depending on fish length. The same objects might therefore have different images and perceptual meaning for fish of different sizes.

Transcutaneous voltages in a given fish will be proportional to the fish's EOD amplitude. The size of the EOD (measured as the electromotive force in air) appears to be relatively independent of fish size (Cox, 1938; Caputi *et al.* 1989, 1993, 1994). However, Knudsen (1975) found that longer fish generate larger EOD fields in the external medium. This results from two features that do depend on fish size: (1) larger fish have lower internal and skin resistances than do small fish, and the current output of the equivalent source is therefore larger; (2) larger fish may be represented by a longer dipole, resulting in a greater field strength at a given distance from the body.

Pre-receptor effects in the generation of the physical electric image

Electroreception, like vision, creates a two-dimensional image of the external three-dimensional space. In vertebrate vision, image formation results from point-to-point central projection of the external visual field onto the retina.

Electroreception implies the projection of a three-dimensional world (which may be represented as a distribution of dipoles) onto the skin of the fish. The rules governing projections in electroreception depend on fish geometry, on the resistance of fish tissues and on water resistivity.

The model suggests that the position of the object is signaled by the point on the skin surface where the absolute value of the transcutaneous voltage is a maximum. This result is consistent with the site of maximal activity of electroreceptors found by Szabo and Hagiwara (1967) and is also consistent with results obtained in other species (Bastian, 1986; Rasnow, 1996). In vision, an object that projects to a particular point in the retina is located on a particular straight line that passes through the retinal point and the optical center of the pre-receptor system. The portion of space covered by all these lines defines the visual field for each eye. In electroreception, a maximum transcutaneous voltage modulation at a given point on the skin indicates that there is an object on a line passing through this point. In this way, we can define an electroreceptive field taking into account the surface of skin containing the electroreceptors and the projecting lines passing through each point on the skin. This mapping rule constitutes the initial clue for object location.

When the head-to-tail EOD is positive, an increase in the resistance of an element of the network, normally oriented to the skin (representing an object), has the same effect as an equivalent dipole with the positive pole facing the fish. Such an object produces a decrease in the outward currents on a given area of skin. The size of this area of skin increases with object distance. This result is similar to that obtained in model (Heiligenberg, 1975) and experimental (Rasnow, 1996) studies of gymnotiforms.

The 'Mexican hat' effect described here and predicted by the conceptual model of Scheich and Bullock (1974) explains the spatial pattern of afferent activity found by Szabo and Hagiwara (1967). This effect may act as a pre-receptor mechanism of contrast enhancement. A large object close to the skin may yield currents with a spatial distribution that is similar to that of the currents produced by a small object far away from the skin. The 'Mexican hat' effect, acting as an edge detector, helps to resolve this ambiguity. Since objects are defined by their boundaries, mechanisms that favor edge detection yield powerful transformations. As a result of the 'Mexican hat' effect, the border of the image of nearby objects appears more clearly than that of distant objects. Therefore, the sharpness of the image provides clues for object distance determination.

As demonstrated by the model (Fig. 7) and the experimental results shown in Fig. 9, the low resistivity of the internal tissues relative to that of water produces a 'shielding effect', separating one side of the fish from the other. The currents generated by the dipole are conducted along the fish body, and the skin of the opposite side is therefore poorly stimulated. This shielding effect provides a third clue for object location.

Nevertheless, object location in three-dimensional space cannot be solved unambiguously by a single two-dimensional image. As in vision, more than one image must be integrated to solve ambiguities. To make this process possible, the images must be generated on different surfaces, on a single moving surface or on a static surface excited from different angles. For static objects, movements of the fish or its tail (containing its EO) will generate different images. Moving objects themselves will generate images from different locations. In addition, moving objects are likely to be animals and, therefore, to be electric sources that can to be sensed by the passive electrosensory system (ampullary electroreceptors) as well as by mormyromast electroreceptors involved in active electrolocation.

In conclusion, our measurements and modeling studies indicate that mormyrids (like gymnotids) have a relatively low skin resistance. This feature results in important filtering effects of both reafferent and exafferent signals. One of these, the 'Mexican hat' effect, constitutes an edge detector mechanism originating in non-neural pre-receptor structures.

The modeling studies suggest a set of rules for understanding electrolocation: (1) the point on the skin where the transcutaneous voltages are maximally modulated indicates the position of the object in the electroreceptive field; (2) the contralateral side is minimally stimulated by an object; (3) sharp modulation with a strong surround effect indicates proximity, while smooth modulation with a poor surround effect indicates remoteness; (4) a modulation of the type center–increase/surround–decrease indicates an object with a higher conductivity than that of the water, while the opposite pattern indicates objects that are more resistive than water. Rasnow (1996) suggested a similar set of rules on the basis of maps of the electric field of *Apteronotus leptorhyncus.*

The authors thank Omar Trujillo-Cenóz for the critical reading and helpful discussion of the manuscript. This research was partially supported by the Commission of the European Communities (contract CI1*-CT92–0085 to R.B., A.C. and K.G.), the Comisión Sectorial de Investigación Científica, Universidad de la República (to R.B.) and the Consejo Nacional de Investigaciones Cientificas y Tecnicas (to R.B.).

References

BACHER, M. (1983). A new method for the simulation of electric fields generated by electric fish and their distortion by objects. *Biol. Cybernetics* **47**, 51–58.

BASTIAN, J. (1986). Electrolocation: behavior, anatomy and physiology. In *Electroreception* (ed. T. H. Bullock and W. Heiligenberg), pp. 577–612. New York: Wiley.

BELL, C. C. (1981). Central distribution of octavolateral afferents and efferents in a teleost (Mormyridae). *J. comp. Neurol.* **195**, 391–414.

BELL, C. C. (1986). Electrorreception in mormyrid fish. Central physiology. In *Electroreception* (ed. T. H. Bullock and W. Heiligenberg), pp. 423–452. New York: Wiley.

BELL, C. C. (1989). Sensory coding and corollary discharge effects in mormyrid electric fish. *J. exp. Biol.* **146**, 229–253.

BELL, C. C. (1990*a*). Mormyromast electroreceptor organs and their afferent fibers in mormyrid fish. II. Intra-axonal recordings show initial stages of central processing. *J. Neurophysiol.* **63**, 303–318.

BELL, C. C. (1990*b*). Mormyromast electroreceptor organs and their afferent fibers in mormyrid fish. III. Physiological differences between two morphological types of fibers. *J. Neurophysiol.* **63**, 319–332.

BELL, C. C., BRADBURY, J. AND RUSSELL, C. (1976). The electric organ of a mormyrid as a current and voltage source. *J. comp. Physiol.* A **110**, 65–88.

BELL, C. C. AND RUSSELL, C. (1978). Effect of electric organ discharge on ampullary receptors in a mormyrid. *Brain Res.* **145**, 85–96.

BELL, C. C. AND SZABO, T. (1986). Electroreception in mormyrid fish. Central anatomy. In *Electroreception* (ed. T. H. Bullock and W. Heiligenberg), pp. 375–421. New York: Wiley.

BENNETT, M. V. L. (1965). Electroreceptors in mormyrids. *Cold Spring Harbor Symp. quant. Biol.* **30**, 245–262.

BENNETT, M. V. L. (1971). Electroreceptors. In *Fish Physiology*, vol. 5 (ed. W. S. Hoar and D. J. Randall), pp. 493–574. New York: Academic Press.

BORGES, J. L. (1967). *Museo, Del Rigor en la Ciencia. In Obras Completas*. Buenos Aires: Emece.

BOUDINOT, M. (1971). Contribution à l'étude des caractéristiques électriques de l'organe effecteur de *Gnathonemus petersii*. Mémoire présenté au Conservatoire National des Arts et Métiers pour obtenir le diplôme d'ingénieur C.N.A.M. Paris, France.

CAPUTI, A. AND BUDELLI, R. (1995). The electric image in weakly electric fish. II. A data based model of waveform generation in *Gymnotus carapo*. *J. comput. Neurosci.* **2**, 131–147.

CAPUTI, A., MACADAR, O. AND TRUJILLO-CENÓZ, O. (1989). Waveform generation of the electric organ discharge in *Gymnotus carapo*. III. The fish's body as an electric source. *J. comp. Physiol.* A **165**, 361–370.

CAPUTI, A., MACADAR, O. AND TRUJILLO-CENÓZ, O. (1994). Waveform generation in *Rhamphichthys rostratus* (L.) (Teleostei, Gymnotiformes). The electric organ and its spatiotemporal activation pattern. *J. comp. Physiol.* A **174**, 633–642.

CAPUTI, A., SILVA, A. AND MACADAR, O. (1993). Electric organ activation in *Gymnotus carapo*: Spinal origin and peripheral mechanisms. *J. comp. Physiol.* A **173**, 227–232.

COOMBS, S., HASTINGS, M. AND FINNERUM, J. (1996). Modeling and measuring lateral line excitatory patterns *J. comp. Physiol.* A **178**, 359–371.

COX, R. T. (1938). The electric eel at home. *N.Y. zool. Soc.* **41**, 59–65.

CRAMER, H. (1960). *Metodos Matematicos de Estadistica*, second edition. Madrid: Aguilar.

GRANT, K., MEEK, J., SUGAWARA, Y., VERON, M., DENIZOT, J. P., HAFMANS, T. G. M., SERRIER, J. AND SZABO, T. (1996). Projection neurons of the mormyrid electrosensory lateral line lobe: morphology, immunohistochemistry and synaptology. *J. comp. Neurol.* **357**, 18–42.

HEILIGENBERG, W. (1973). Electrolocation of objects in the electric fish *Eigenmannia* (Rhamphichthyidae, Gymnotoidei). *J. comp. Physiol.* A **103**, 247–272.

HEILIGENBERG, W. (1975). Theoretical and experimental approaches to spatial aspects of electrolocation. *J. comp. Physiol.* A **103**, 247–272.

HOPKINS, C. D. (1981). On the diversity of electric signals in a community of mormyrids electric fish in West Africa. *Am. Zool.* **21**, 211–222.

HOPKINS, C. D. (1983). Functions and mechanisms in electroreception. In *Fish Neurobiology* (ed. R. G. Northcutt and R. Davis), pp. 215–259. Ann Arbor: University of Michigan Press.

HOSHIMIYA, N., SHOGEN, K., MATSUO, T. AND CHICHIBU, S. (1980). The *Apteronotus* EOD field: Waveform and EOD field simulation. *J. comp. Physiol.* A **135**, 283–290.

KEIDEL, W. D. (1984). The sensory detection of vibrations. In *Foundations of Sensory Sciences* (ed. W. W. Dowson and J. M. Enoch), pp. 465–512. Berlin: Springer-Verlag.

KNUDSEN, E. (1975). Spatial aspects of the electric fields generated by weakly electric fish. *J. comp. Physiol.* A **99**, 103–118.

LISSMANN, H. W. AND MACHIN, K. E. (1958). The mechanism of object location in *Gymnarchus niloticus* and similar fish. *J. exp. Biol.* **35**, 451–486.

MARR, D. (1982). *Vision*. Cambridge, MA: MIT Press.

MEEK, J. AND GRANT, K. (1994). The role of motor command feedback in electrosensory processing. *Eur. J. Morph.* **32**, 225–234.

MEEK, J., GRANT, K., SUGAWARA, Y., HAFMANS, T. G. M., VERON, M. AND DENIZOT, J. P. (1996). Interneurons of the ganglionic layer of the mormyrid electrosensory lateral line lobe: morphology, immunohistochemistry and synaptology. *J. comp. Neurol.* **357**, 43–65.

MEYER, J. H. (1982). Behavioral responses of weakly electric fish to complex impedances. *J. comp. Physiol.* A **145**, 459–470.

MOLLER, P. (1995). EOD diversity in Mormyridae. In *Electric Fishes, History and Behaviour* (ed. T. J. Pitcher and P. Hart), pp. 180–190. London: Chapman & Hall.

QUINET, P. (1971). Etude systématique des organes sensoriels de la peau des Mormyriformes (Pisces, Mormyriformes). *Annls Musée Royal Afrique Centrale, Tervuren (Belgium) Series 8* **190**, 1–97.

RASNOW, B. (1996). The effects of simple objects on the electric field of *Apteronotus. J. comp. Physiol.* A **178**, 397–411.

RASNOW, B., ASSAD, C. AND BOWER, J. M. (1993). Phase and amplitude maps of the electric organ discharge of the weakly electric fish *Apteronotus leptorhynchus. J. comp. Physiol.* A **172**, 481–491.

RASNOW, B. AND BOWER, J. M. (1996). The electric organ discharges of the gymnotiform fishes. I. *Apteronotus leptorhynchus*. *J. comp. Physiol.* A **178**, 383–396.

SCHEICH, H. AND BULLOCK, T. H. (1974). The role of electroreceptors in the animal's life. II. The detection of electric fields from electric organs. In *Handbook of Sensory Physiology*, vol. III/3 (ed. A. Fessard), pp. 201–256. Berlin: Springer Verlag.

SZABO, T. AND FESSARD, A. (1974). Physiology of electroreceptors. In *Handbook of Sensory Physiologyy*, vol. III/3 (ed. A. Fessard), pp. 60–124. Berlin: Springer Verlag.

SZABO, T. AND HAGIWARA, S. (1967). A latency change mechanism involved in sensory coding of electric fish. *Physiol. Behav.* **2**, 331–335.

VON DER EMDE, G. (1991). Discrimination of objects through electrolocation in the weakly electric fish, *Gnathonemus petersii*. *J. comp. Physiol.* A **167**, 413–421.

VON DER EMDE, G. (1993). The sensing of electrical capacitance by weakly electric mormyrid fish: effect of water conductivity. *J. exp. Biol.* **181**, 157–173.

VON DER EMDE, G. AND BLECKMANN, H. (1992). Differential responses of two types of afferents to signal distortions may permit capacitance measurements in weakly electric fish, *Gnathonemus petersii*. *J. comp. Physiol.* A **167**, 413–421.

ZIPSER, B. AND BENNETT, M. V. L. (1976*a*). Responses of cells of the posterior lateral line lobe to activation of electroreceptors in a mormyrid fish. *J. Neurophysiol.* **39**, 693–712.

ZIPSER, B. AND BENNETT, M. V. L. (1976*b*). Interaction of electrosensory and electromotor signals in the lateral line lobe of a mormyrid fish. *J. Neurophysiol.* **39**, 713–721.